Micro-Station - Modal Analysis

Dehaeze Thomas

October 24, 2024

Contents

In order to further improve the accuracy of the performance predictions, a model that better represents the micro-station dynamics is required. A multi-body model, consisting of several rigid bodies connected by kinematic constraints (i.e. joints), springs and damper elements, is a good candidate to model the micro-station.

Even though the inertia of each solid body can easily be estimated from its geometry and its material density, it is more difficult to properly estimate the stiffness and damping properties of the guiding elements connecting each solid body. The experimental modal analysis will be use to tune the model, and to verify that a multi-body model can represent accurately the dynamics of the micro-station.

The approach of tuning the multi-body model from measurements is illustrated in Figure 1. First, a *response model* is obtained, which corresponds to a set of frequency response functions computed from experimental measurements. From this response model, and modal model can be computed, which consists of two matrices: one containing the natural frequencies and damping factors of the considered modes, and another one describing the mode shapes. This modal model can then be used to tune the spatial model (i.e. the multi-body model), that is to say to tune the mass of the considering solid bodies, and the springs and dampers connecting the solid bodies.

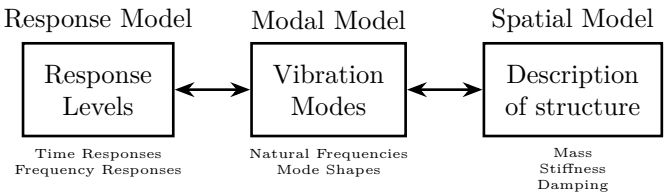

Figure 1: Figure caption

The measurement setup used to obtain the response model is presented in Section 1. This includes the instrumentation used (i.e. instrumented hammer, accelerometers and acquisition system), the test planing, and a first analysis of the obtained signals.

In Section 2, the obtained frequency response functions between the forces applied using the instrumented hammer and the various accelerometers fixed to the structure are computed. These measurements are projected at the center of mass of each considered solid body to ease the further use of the results. The solid body assumption is then verified, validating the use of the multi-body model.

Finally, the modal analysis is performed in Section 3. It shows how complex the micro-station dynamics is, and the necessity of the developed more complex multi-body model.

1 Measurement Setup

In order to perform an experimental modal analysis, a proper measurement setup is key. This include using appropriate instrumentation (presented in Section 1.1) and properly preparing the structure to be measured (Section 1.2). Then, the location of the measured motion (Section 1.3) and the location of the hammer impacts (Section 1.4) have to be chosen carefully. Obtained force and acceleration signals are shown in Section 1.5, and the quality of the measured data is checked.

1.1 Used Instrumentation

Three equipment are key to perform a good modal analysis. First, *accelerometers* are used to measure the response of the structure. Here, 3-axis accelerometers[1] shown in figure 1.1a are used. These accelerometers are glued to the micro-station using a thin layer of wax for best results [1, chapt. 3.5.7].

(a) 3-axis accelerometer

(b) Instrumented hammer

(c) OROS acquisition system

Figure 1.1: Instrumentation used for the modal analysis

Then, an *instrumented hammer*[2] (figure 1.1b) is used to apply forces to the structure in a controlled way. Tests have been conducted to determine the most suitable hammer tip (ranging from a metallic one to a soft plastic one). The softer tip has been found to give best results as it injects more energy in the low frequency range where the coherence was low, such that the overall coherence was improved.

Finally, an *acquisition system*[3] (figure 1.1c) is used to acquire the injected force and the response

[1] PCB 356B18. Sensitivity is $1\,V/g$, measurement range is $\pm 5\,g$ and bandwidth is 0.5 to 5 kHz.
[2] Kistler 9722A2000. Sensitivity of $2.3\,mV/N$ and measurement range of $2\,kN$
[3] OROS OR36. 24bits signal-delta ADC.

accelerations in a synchronized way and with sufficiently low noise.

1.2 Structure Preparation and Test Planing

In order to obtain meaningful results, the modal analysis of the micro-station in performed *in-situ*. To do so, all the micro-station stage controllers are turned "ON". This is especially important for stages for which the stiffness is provided by local feedback control, which is case for the air bearing spindle, and the translation stage. If these local feedback control were turned OFF, this would have resulted in very low frequency modes difficult to measure in practice, and this would also have lead to decoupled dynamics which would not be the case in practice.

The top part representing the active stabilization stage has been disassembled as the active stabilization stage and the sample will be added in the multi-body model afterwards.

To perform the modal-analysis from the measured responses, the $n \times n$ frequency response function matrix $\mathbf{H}$ needs to be measured, where n is the considered number of degrees of freedom. The H_{jk} element of this Frequency Response Function (FRF) matrix corresponds to the frequency response function from a force F_k applied at Degree of freedom (DoF) k to the displacement of the structure X_j at DoF j. Measuring this FRF matrix is very time consuming as it requires to make n^2 measurements. However thanks to the principle of reciprocity ($H_{jk} = H_{kj}$) and using the *point measurement* (H_{jj}), it is possible to reconstruct the full matrix by measuring only one column or one line of the matrix $\mathbf{H}$ [1, chapt. 5.2]. Therefore, a minimum set of n frequency response functions needs to be measured. This can be done either by measuring the response X_j at a fixed DoF j while applying forces F_i for at all n considered DoF, or by applying a force F_k at a fixed DoF k and measuring the response X_i for all n DoF.

It is however not advised to measure only one row or one column as one or more modes may be missed by an unfortunate choice of force or acceleration measured locations (for instance if the force is applied at a vibration node of a particular mode). In this modal-analysis, it is chosen to measure the response of the structure at all considered DoF, and to excite the structure at one location in three directions in order to have some redundancy and to make sure that all modes are properly energized.

1.3 Location of the Accelerometers

The location of the accelerometers fixed to the micro-station is essential as it defines where the dynamics is measured. A total of 23 accelerometers are fixed to the six key stages of the micro station: the lower and upper granites, the translation stage, the tilt stage, the spindle and the micro hexapod. The position of the accelerometers are visually shown on a CAD model in Figure 1.2 and their precise locations with respect to a frame located at the point of interest are summarized in Table 1.1. Pictures of the accelerometers fixed to the translation stage and to the micro-hexapod are shown in Figure 1.3.

As all key stages of the micro-station are foreseen to behave as solid bodies, only 6 DoF can be considered per solid body. However, it was chosen to use four 3-axis accelerometers (i.e. 12 measured DoF) for each considered solid body to have some redundancy and to be able to verify the solid body assumption (see Section 2.2).

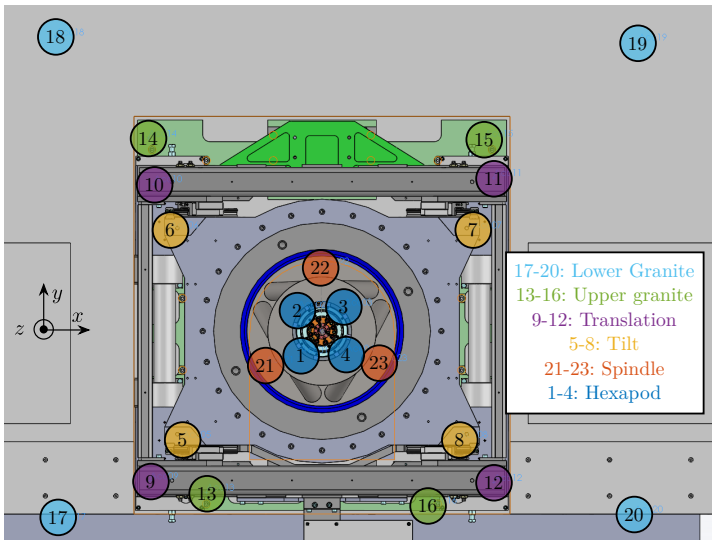

Figure 1.2: Position of the accelerometers

Table 1.1: Positions in mm

	x	y	z
Low. Granite	-730	-526	-951
Low. Granite	-735	814	-951
Low. Granite	875	799	-951
Low. Granite	865	-506	-951
Up. Granite	-320	-446	-786
Up. Granite	-480	534	-786
Up. Granite	450	534	-786
Up. Granite	295	-481	-786
Translation	-475	-414	-427
Translation	-465	407	-427
Translation	475	424	-427
Translation	475	-419	-427
Tilt	-385	-300	-417
Tilt	-420	280	-417
Tilt	420	280	-417
Tilt	380	-300	-417
Spindle	-155	-90	-594
Spindle	0	180	-594
Spindle	155	-90	-594
Hexapod	-64	-64	-270
Hexapod	-64	64	-270
Hexapod	64	64	-270
Hexapod	64	-64	-270

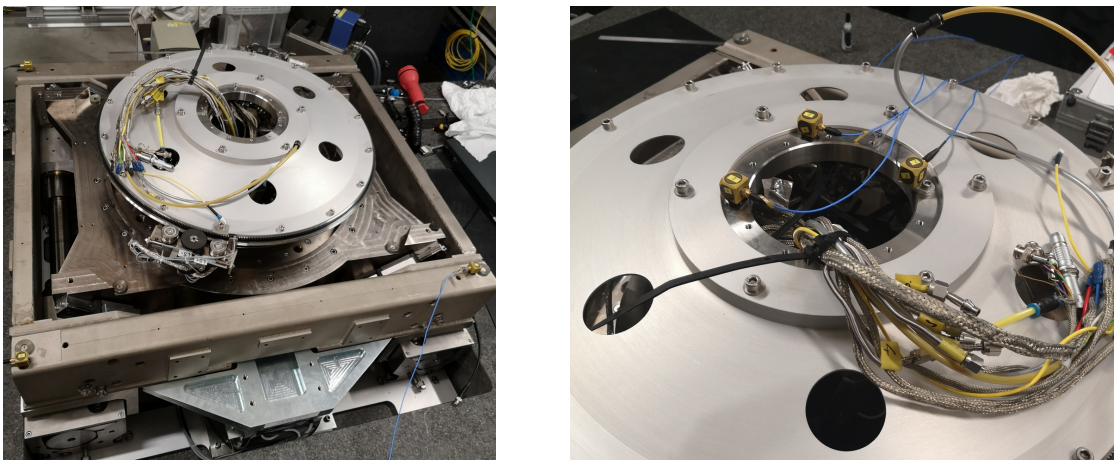

(a) T_y stage **(b)** Micro-Hexapod

Figure 1.3: Accelerometers fixed on the micro-station stages

1.4 Hammer Impacts

The chosen location of the hammer impact corresponds to the location of accelerometer number 11 fixed to the translation stage. It was chosen to match the location of one accelerometer, because a *point measurement* (i.e. a measurement of H_{kk}) is necessary to be able to reconstruct the full FRF matrix [1].

The impacts are performed in three directions, which are shown in figures 1.4a, 1.4b and 1.4c. This excitation point with the three considered directions allows to properly energize all the modes in the

frequency band of interest and to provide good coherence for all the accelerometers as will be shown in the next section.

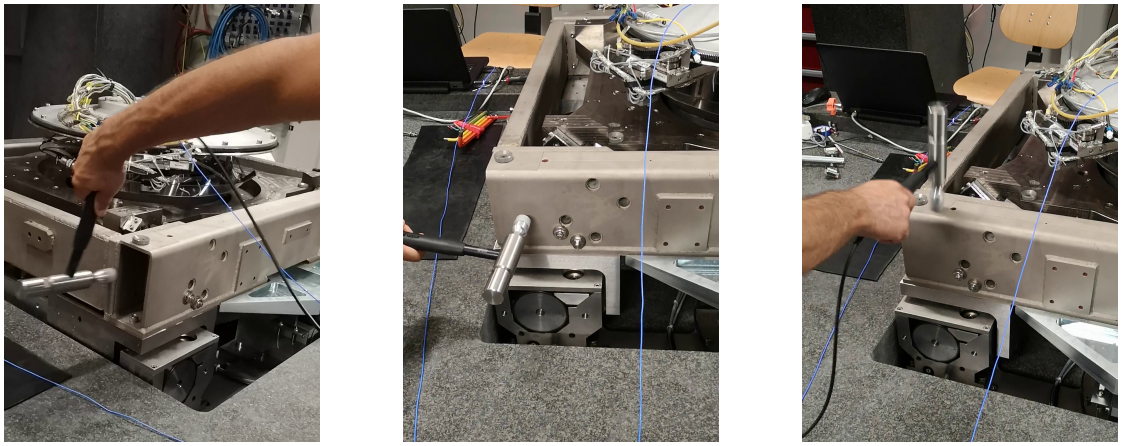

(a) X impact **(b)** Y impact **(c)** Z impact

Figure 1.4: The three hammer impacts used for the modal analysis

1.5 Force and Response signals

The force sensor of the instrumented hammer and the accelerometers signals are shown in the time domain in Figure 1.5a. Sharp "impacts" can be seen for the force sensor, indicating wide frequency band excitation. For the accelerometer, a much more complex signal can be observed, indicating complex dynamics.

The "normalized" Amplitude Spectral Density (ASD) of the two signals are computed and shown in Figure 1.5b. Conclusions based on the time domain signals can be clearly seen in the frequency domain (wide frequency content for the force signal and complex dynamics for the accelerometer).

The frequency response function H_{jk} from the applied force F_k to the measured acceleration X_j is then computed and shown Figure 1.6a. The quality of the obtained data can be estimated using the *coherence* function, which is shown in Figure 1.6b. Good coherence is obtained from 20 Hz to 200 Hz which corresponds to the frequency range of interest.

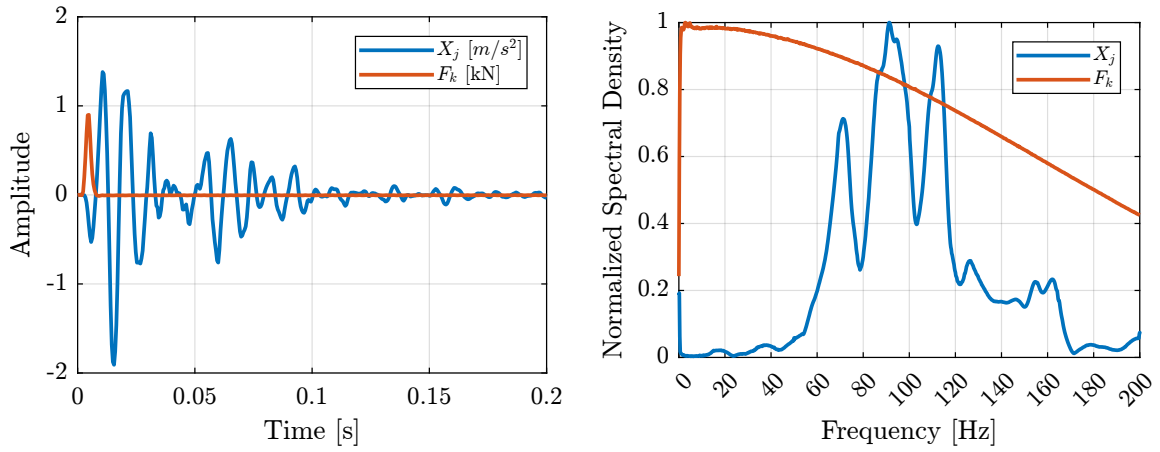

(a) Time domain signals

(b) Amplitude Spectral Density (normalized)

Figure 1.5: Raw measurement of the acceleromter (blue) and of the force sensor at the Hammer tip (red) (a). Computed Amplitude Spectral Density of the two signals (normalized) (b)

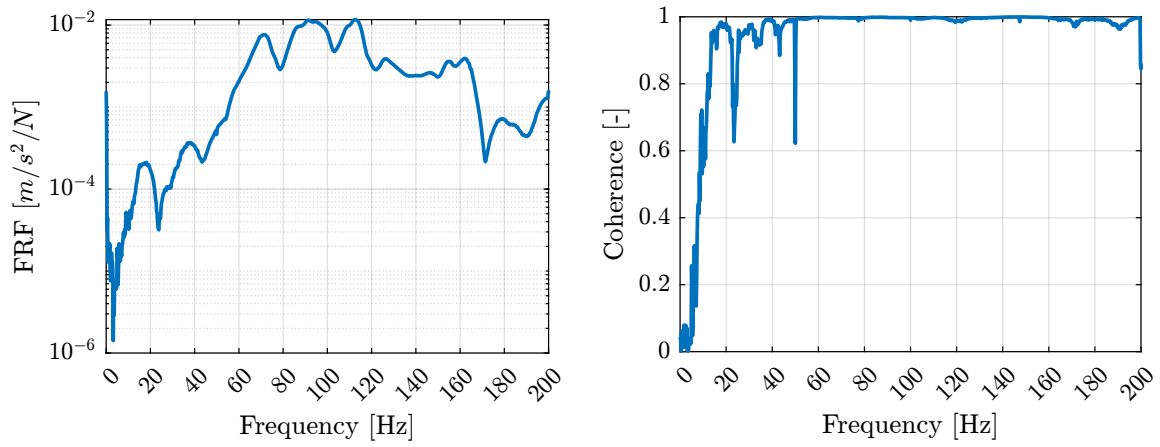

(a) Frequency Response Function

(b) Coherence

Figure 1.6: Computed frequency response function from the applied force F_k and the measured response X_j (a) as well as computed coherence (b)

2 Frequency Analysis

All measurements where conducted and a $n \times p \times q$ Frequency Response Functions Matrix were computed with:

- $n = 69$: the number of output measured accelerations (23 3-axis accelerometers)
- $p = 3$: the number of input force excitations
- $q = 801$: the number of frequency points ω_i

For each frequency point ω_i, a 2D complex matrix is obtained that links the 3 force inputs to the 69 output accelerations (2.1).

$$\mathbf{H}(\omega_i) = \begin{bmatrix} \frac{D_{1_x}}{F_x}(\omega_i) & \frac{D_{1_x}}{F_y}(\omega_i) & \frac{D_{1_x}}{F_z}(\omega_i) \\ \frac{D_{1_y}}{F_x}(\omega_i) & \frac{D_{1_y}}{F_y}(\omega_i) & \frac{D_{1_y}}{F_z}(\omega_i) \\ \frac{D_{1_z}}{F_x}(\omega_i) & \frac{D_{1_z}}{F_y}(\omega_i) & \frac{D_{1_z}}{F_z}(\omega_i) \\ \frac{D_{2_x}}{F_x}(\omega_i) & \frac{D_{2_x}}{F_y}(\omega_i) & \frac{D_{2_x}}{F_z}(\omega_i) \\ \vdots & \vdots & \vdots \\ \frac{D_{23_z}}{F_x}(\omega_i) & \frac{D_{23_z}}{F_y}(\omega_i) & \frac{D_{23_z}}{F_z}(\omega_i) \end{bmatrix} \tag{2.1}$$

However, for the multi-body model being developed, only 6 solid bodies are considered, namely: the bottom granite, the top granite, the translation stage, the tilt stage, the spindle and the hexapod. Therefore, only $6 \times 6 = 36$ degrees of freedom are of interest. The objective in this section is therefore to process the Frequency Response Matrix to reduce the number of measured DoF from 69 to 36.

The coordinate transformation from accelerometers DoF to the solid body 6 DoFs (three translations and three rotations) is performed in Section 2.1. The $69 \times 3 \times 801$ frequency response matrix is then reduced to a $36 \times 3 \times 801$ frequency response matrix where the motion of each solid body is expressed with respect to its center of mass.

To validate this reduction of DoF and the solid body assumption, the frequency response function at the accelerometer location are recomputed from the reduced frequency response matrix and are compared with the initial measurements in Section 2.2.

2.1 From accelerometer DOFs to solid body DOFs

Let's consider the schematic shown in Figure 2.1 where the motion of a solid body is measured at 4 distinct locations (in x, y and z directions). The goal here is to link these $4 \times 3 = 12$ measurements to the 6 DoF of the solid body expressed in the frame $\{O\}$.

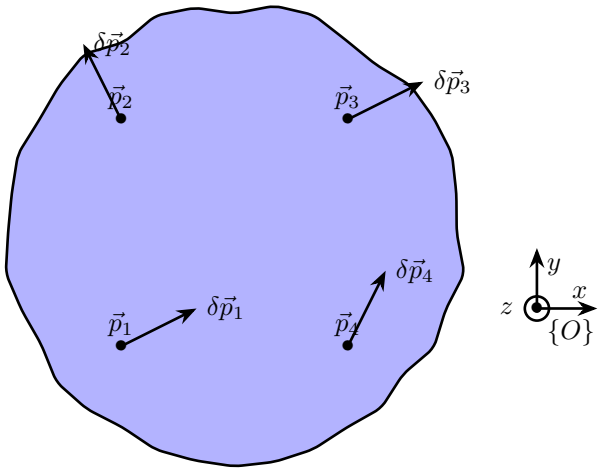

Figure 2.1: Schematic of the measured motions of a solid body

Writing Eq. (**??**) for the four displacement sensors in a matrix form gives (2.2).

$$\left[\begin{array}{ccc|ccc} 1 & 0 & 0 & 0 & p_{1z} & -p_{1y} \\ 0 & 1 & 0 & -p_{1z} & 0 & p_{1x} \\ 0 & 0 & 1 & p_{1y} & -p_{1x} & 0 \\ \hline & \vdots & & & \vdots & \\ \hline 1 & 0 & 0 & 0 & p_{4z} & -p_{4y} \\ 0 & 1 & 0 & -p_{4z} & 0 & p_{4x} \\ 0 & 0 & 1 & p_{4y} & -p_{4x} & 0 \end{array}\right] \left[\begin{array}{c} \delta p_x \\ \delta p_y \\ \delta p_z \\ \hline \delta\Omega_x \\ \delta\Omega_y \\ \delta\Omega_z \end{array}\right] = \left[\begin{array}{c} \delta p_{1x} \\ \delta p_{1y} \\ \delta p_{1z} \\ \hline \vdots \\ \hline \delta p_{4x} \\ \delta p_{4y} \\ \delta p_{4z} \end{array}\right] \tag{2.2}$$

Provided that the four sensors are properly located, the system of equation (2.2) can be solved by matrix inversion. The motion of the solid body expressed in a chosen frame $\{O\}$ can be determined using equation (2.3). Note that this matrix inversion is equivalent to resolving a mean square problem. Therefore, having more accelerometers permits to have a better approximation of the motion of the solid body.

$$\left[\begin{array}{c} \delta p_x \\ \delta p_y \\ \delta p_z \\ \hline \delta\Omega_x \\ \delta\Omega_y \\ \delta\Omega_z \end{array}\right] = \left[\begin{array}{ccc|ccc} 1 & 0 & 0 & 0 & p_{1z} & -p_{1y} \\ 0 & 1 & 0 & -p_{1z} & 0 & p_{1x} \\ 0 & 0 & 1 & p_{1y} & -p_{1x} & 0 \\ \hline & \vdots & & & \vdots & \\ \hline 1 & 0 & 0 & 0 & p_{4z} & -p_{4y} \\ 0 & 1 & 0 & -p_{4z} & 0 & p_{4x} \\ 0 & 0 & 1 & p_{4y} & -p_{4x} & 0 \end{array}\right]^{-1} \left[\begin{array}{c} \delta p_{1x} \\ \delta p_{1y} \\ \delta p_{1z} \\ \hline \vdots \\ \hline \delta p_{4x} \\ \delta p_{4y} \\ \delta p_{4z} \end{array}\right] \tag{2.3}$$

From the CAD model, the position of the center of mass of each considered solid body is computed (see Table 2.1). Then, the position of each accelerometer with respect to the center of mass of the corresponding solid body can easily be derived.

Using (2.3), the frequency response matrix $\mathbf{H}_{\text{CoM}}$ (2.4) expressing the response at the center of mass of each solid body D_i (i from 1 to 6 for the 6 considered solid bodies) can be computed from the initial FRF matrix $\mathbf{H}$.

Table 2.1: Center of mass of considered solid bodies with respect to the "point of interest"

	X [mm]	Y [mm]	Z [mm]
Bottom Granite	45	144	-1251
Top granite	52	258	-778
Translation stage	0	14	-600
Tilt Stage	0	-5	-628
Spindle	0	0	-580
Hexapod	-4	6	-319

$$\mathbf{H}_{\text{CoM}}(\omega_i) = \begin{bmatrix} \frac{D_{1,T_x}}{F_x}(\omega_i) & \frac{D_{1,T_x}}{F_y}(\omega_i) & \frac{D_{1,T_x}}{F_z}(\omega_i) \\ \frac{D_{1,T_y}}{F_x}(\omega_i) & \frac{D_{1,T_y}}{F_y}(\omega_i) & \frac{D_{1,T_y}}{F_z}(\omega_i) \\ \frac{D_{1,T_z}}{F_x}(\omega_i) & \frac{D_{1,T_z}}{F_y}(\omega_i) & \frac{D_{1,T_z}}{F_z}(\omega_i) \\ \frac{D_{1,R_x}}{F_x}(\omega_i) & \frac{D_{1,R_x}}{F_y}(\omega_i) & \frac{D_{1,R_x}}{F_z}(\omega_i) \\ \frac{D_{1,R_y}}{F_x}(\omega_i) & \frac{D_{1,R_y}}{F_y}(\omega_i) & \frac{D_{1,R_y}}{F_z}(\omega_i) \\ \frac{D_{1,R_z}}{F_x}(\omega_i) & \frac{D_{1,R_z}}{F_y}(\omega_i) & \frac{D_{1,R_z}}{F_z}(\omega_i) \\ \frac{D_{2,T_x}}{F_x}(\omega_i) & \frac{D_{2,T_x}}{F_y}(\omega_i) & \frac{D_{2,T_x}}{F_z}(\omega_i) \\ \vdots & \vdots & \vdots \\ \frac{D_{6,R_z}}{F_x}(\omega_i) & \frac{D_{6,R_z}}{F_y}(\omega_i) & \frac{D_{6,R_z}}{F_z}(\omega_i) \end{bmatrix} \tag{2.4}$$

2.2 Verification of solid body assumption

From the response of one solid body along its 6 DoFs (i.e. from $\mathbf{H}_{\text{CoM}}$), and using equation (2.2), it is possible to compute the response of the same solid body at any considered position. In particular, the response at the location of the four accelerometers can be computed. Comparing the computed response of a particular accelerometer from $\mathbf{H}_{\text{CoM}}$ with the original measurements $\mathbf{H}$ is use to check if solid body assumption is correct in the frequency band of interest.

The comparison is made for the 4 accelerometers fixed to the micro-hexapod (Figure 2.2). The original frequency response functions and the ones computed from the CoM responses are well matching in the frequency range of interested. Similar results are obtained for the other solid bodies, indicating that the solid body assumption is valid, and that a multi-body model can be used to represent the dynamics of the micro-station. This also validates the reduction of the number of degrees of freedom from 69 (23 accelerometers with each 3 DoF) to 36 (6 solid bodies with 6 DoF).

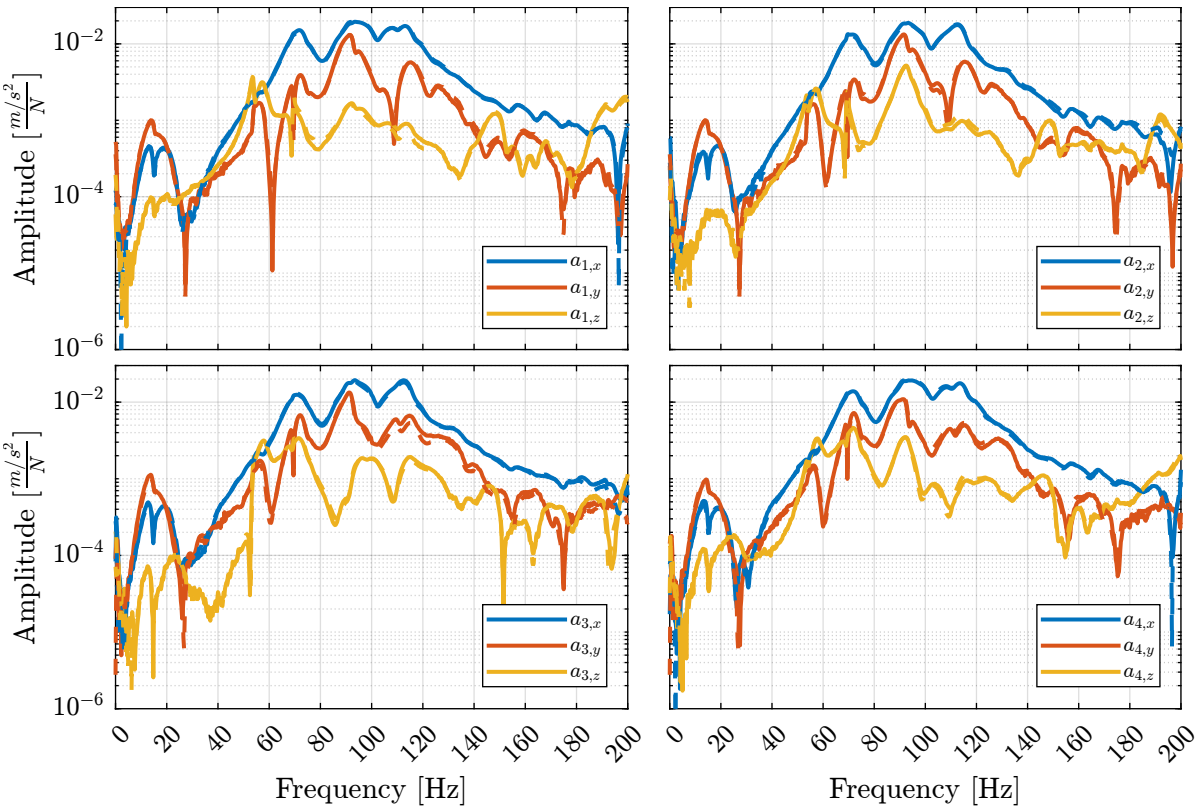

Figure 2.2: Comparaison of the original accelerometer response (solid curves) and reconstructed response from the solid body response (dashed curves). For accelerometers 1 to 4 corresponding to the micro-hexapod.

3 Modal Analysis

The goal here is to extract the modal parameters describing the modes of station being studied, namely the natural frequencies and the modal damping (i.e. the eigenvalues) and the mode shapes (.i.e. the eigenvectors). This is done from the FRF matrix previously extracted from the measurements.

In order to perform the modal parameter extraction, the order of the modal model needs to be estimated (i.e. the number of modes in the frequency band of interest). This is done using the Mode Indicator Functions (MIF) in section 3.1.

In section 3.2, the modal parameter extraction is performed. Graphical display of the mode shapes can be computed from the modal model, which is quite quite useful to have a physical interpretation of the modes.

To validate the quality of the modal model, the full FRF matrix is computed from the modal model and compared with the initial measured FRF (section 3.3).

3.1 Determine the number of modes

The MIF is here applied to the $n \times p$ FRF matrix where n is a relatively large number of measurement DOFs (here $n = 69$) and p is the number of excitation DOFs (here $p = 3$).

The complex modal indication function is defined in equation (3.1) where Σ is obtained from a SVD of the FRF matrix (3.2).

$$[CMIF(\omega)]_{p\times p} = [\Sigma(\omega)]^T_{p\times n}[\Sigma(\omega)]_{n\times p} \tag{3.1}$$

$$[H(\omega)]_{n\times p} = [U(\omega)]_{n\times n}[\Sigma(\omega)]_{n\times p}[V(\omega)]^H_{p\times p} \tag{3.2}$$

The MIF therefore yields to p values that are also frequency dependent. A peak in the MIF plot indicates the presence of a mode. Repeated modes can also be detected by multiple singular values are having peaks at the same frequency. The obtained MIF is shown on Figure 3.1. A total of 16 modes are found between 0 and 200 Hz. The obtained natural frequencies and associated modal damping are summarized in Table 3.1.

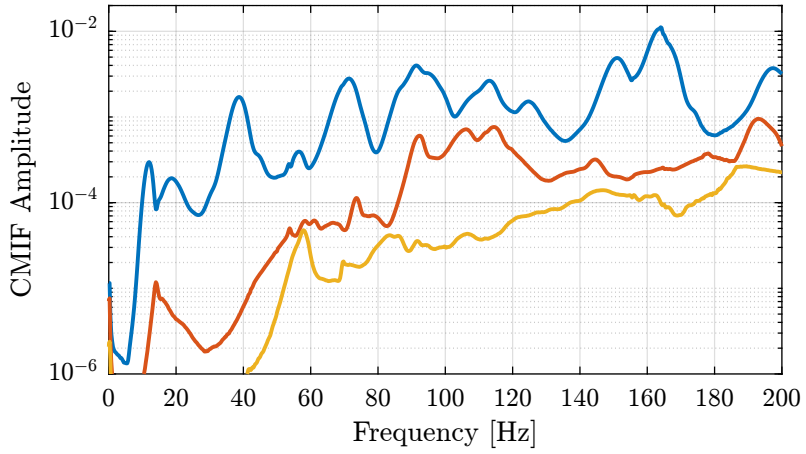

Figure 3.1: Modal Indication Function

Table 3.1: Natural frequencies and modal damping

Mode	Freq. [Hz]	Damp. [%]
1	11.9	12.2
2	18.6	11.7
3	37.8	6.2
4	39.1	2.8
5	56.3	2.8
6	69.8	4.3
7	72.5	1.3
8	84.8	3.7
9	91.3	2.9
10	105.5	3.2
11	106.6	1.6
12	112.7	3.1
13	124.2	2.8
14	145.3	1.3
15	150.5	2.4
16	165.4	1.4

3.2 Modal parameter extraction

The modal identification generally consists of curve-fitting a theoretical expression for an individual FRF to the actual measured data. However, there are multiple level of complexity, from fitting of a single resonance, a complete curve encompassing several resonances and working on a set of many FRF plots all obtained from the same structure.

Here, the last method is used as it gives a unique and consistent model as direct output. It takes into account the fact the the properties of all the individual curves are related by being from the same structure: all FRF plots on a given structure should indicate the same values for the natural frequencies and damping factor of each mode.

From the obtained modal parameters, the mode shapes are computed and can be displayed in the form of animations. Three mode shapes are shown in Figure 3.2.

These animations are quite useful to easily get a better understanding of the system. For instance, the mode shape of the first mode at 11Hz (figure 3.2a) indicates that there is an issue with the lower granite. It turns out that four *Airloc Levelers* are used to level the lower granite (figure 3.3). These are difficult to tune so that the granite is well supported by four of them and not "wobbly" on just two of them.

The modal parameter extraction is made using a proprietary software[1]. For each mode r (from 1 to the number of considered modes $m = 16$), it outputs the frequency ω_r, the damping ratio ξ_r, the eigenvectors $\{\phi_r\}$ (vector of complex numbers with a size equal to the number of measured DoF $n = 69$, see equation (3.3)) and a scaling factor a_r.

$$\{\phi_i\} = \left\{\phi_{i,1_x} \quad \phi_{i,1_y} \quad \phi_{i,1_z} \quad \phi_{i,2_x} \quad \dots \quad \phi_{i,23_z}\right\}^T \tag{3.3}$$

The eigenvalues s_r and s_r^* can then be computed from (3.4).

[1] NVGate software from OROS company

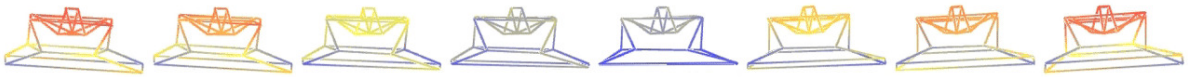

(a) 1^{st} mode at 11.9 Hz: tilt suspension mode of the granite

(b) 6^{th} mode at 69.8 Hz: vertical resonance of the spindle

(c) 13^{th} mode at 124.2 Hz: lateral micro-hexapod resonance

Figure 3.2: Three obtained mode shape animations

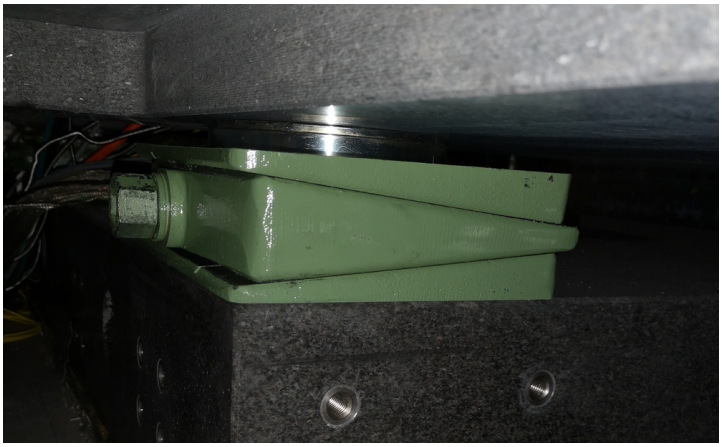

Figure 3.3: AirLoc used for the granite (2120-KSKC)

$$s_r = \omega_r(-\xi_r + i\sqrt{1-\xi_r^2}), \quad s_r^* = \omega_r(-\xi_r - i\sqrt{1-\xi_r^2}) \tag{3.4}$$

3.3 Verify the validity of the Modal Model

In order to check the validity of the modal model, the complete $n \times n$ FRF matrix $\mathbf{H}_{\text{syn}}$ is first synthesized from the modal parameters. Then, the elements of this FRF matrix $\mathbf{H}_{\text{syn}}$ that were already measured can be compared with the measured elements $\mathbf{H}$. New measurements may be performed to compare with elements of the synthesized FRF matrix that were not initialized measured to build the modal model.

In order to synthesize the full FRF matrix, the eigenvectors ϕ_r are first reorganized in a matrix from as shown in equation (3.5).

$$\Phi = \begin{bmatrix} \phi_1 & \dots & \phi_N & \phi_1^* & \dots & \phi_N^* \end{bmatrix}_{n \times 2m} \tag{3.5}$$

The full FRF matrix $\mathbf{H}_{\text{syn}}$ can be synthesize using (3.6).

$$[\mathbf{H}_{\text{syn}}(\omega)]_{n\times n} = [\Phi]_{n\times 2m}[\mathbf{H}_{\text{mod}}(\omega)]_{2m\times 2m}[\Phi]^T_{2m\times n} \tag{3.6}$$

With $\mathbf{H}_{\text{mod}}(\omega)$ a diagonal matrix representing the response of the different modes (3.7).

$$\mathbf{H}_{\text{mod}}(\omega) = \text{diag}\left(\frac{1}{a_1(j\omega - s_1)}, \dots, \frac{1}{a_m(j\omega - s_m)}, \frac{1}{a_1^*(j\omega - s_1^*)}, \dots, \frac{1}{a_m^*(j\omega - s_m^*)}\right)_{2m\times 2m} \tag{3.7}$$

The comparison between the original measured frequency response function and the synthesized one from the modal model is done in Figure 3.4. The match is rather good considering the complex dynamics and the different directions considered.

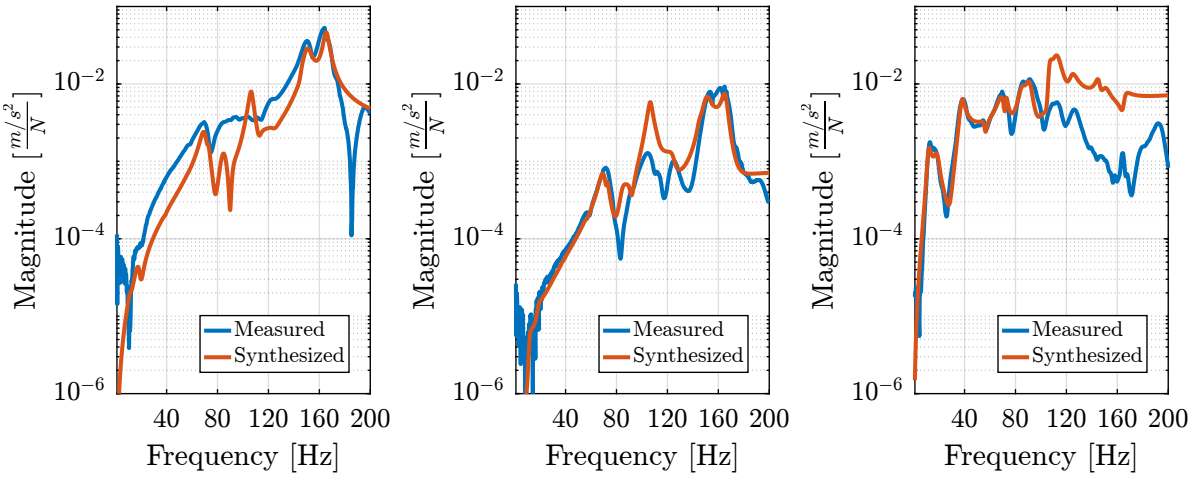

(a) From $F_{11,z}$ to $a_{11,z}$ **(b)** From $F_{11,z}$ to $a_{15,z}$ **(c)** From $F_{11,y}$ to $a_{2,x}$

Figure 3.4: Comparison of the measured FRF with the synthesized FRF from the modal model.

4 Conclusion

In this study, a modal analysis of the micro-station was performed. Thanks to adequate choice of instrumentation and proper set of measurements, high quality frequency response functions could be obtained. As could be expected from a heavy stacked stages architecture, the obtained frequency response functions indicate that the dynamics of the micro-station is complex. It shows lots of coupling between stages and different directions, as well as many modes with various damping properties.

By measuring 12 degrees of freedom on each "stage", it could be verified that in the frequency range of interest, each stage is behaving as a rigid body. This confirms that a solid-body model can be used to properly model the micro-station.

Even though lots of efforts were put in the proper modal analysis of the micro-station, it was stiff very difficult to obtain an accurate modal model. Yet, the measurements will be quite useful when tuning the parameters of the multi-body model.

Bibliography

[1] D. Ewins, *Modal testing: theory, practice and application*. Baldock, Hertfordshire, England Philadelphia, PA: Wiley-Blackwell, 2000, pp. 978–0 863 802 188.

Acronyms

Notation	Description
ASD	Amplitude Spectral Density
DoF	Degree of freedom
FRF	Frequency Response Function
MIF	Mode Indicator Functions
SVD	Singular Value Decomposition